Imaginary part of the infrared conductivity of a $d_{x^2-y^2}$ superconductor

C. Jiang, E. Schachinger, J. P. Carbotte, D. Basov, and T. Timusk

Department of Physics and Astronomy, McMaster University, Hamilton, Ontario, Canada L8S 4M1

(Received 25 September 1995)

We give results for the effect of Born and of resonant impurity scattering on the imaginary part of the infrared conductivity $\sigma(\Omega)$ of a $d_{x^2-y^2}$ superconductor. Inelastic scattering is included in our work through an electron-boson spectral density which also causes the pairing. We emphasize the product of Ω times the imaginary past of $\sigma(\Omega)$. Its zero frequency limit gives the penetration depth, while around twice the gap value it shows smooth behavior as is observed in YBa$_2$Cu$_3$O$_{6.95}$, which has $d_{x^2-y^2}$ symmetry. This is in sharp contrast to the case of an s-wave superconductor which would display a sharp characteristic dip at this energy as seen in BaKBiO. [S0163-1829(96)10026-6]

I. INTRODUCTION

Optical conductivity measurements in the infrared can give valuable information[1,2] about the properties of the low lying charge excitations in metallic systems. In particular, in conventional superconductors, measurements of the real part of the conductivity, which describes the absorption, have given a measure of the size of the superconducting energy gap. While conventional superconductors display an s-wave gap and are in the dirty limit, the high-T_c copper oxides are different. Not only do they have much higher values for their critical temperature T_c, but their coherence length is sufficiently small that they usually fall in the clean rather than in the dirty limit. A feature of the oxides different from the conventional case, and which is not in dispute, is the fact that, at T_c, the inelastic scattering rate is very large and of the order of T_c (Refs. 1 and 2) itself. Further, while the symmetry of the gap is not yet unambiguously established, it is clear that it is not isotropic s-wave. Many experimental data, including optical conductivity results, are consistent with a d-wave order parameter, belonging to[3–15] the $d_{x^2-y^2}$ irreducible representation of the two-dimensional CuO$_2$ tetragonal lattice. Of these various experiments, however, many require only that the gap goes through zero[8–15] at points on the Fermi surface and such experiments do not probe directly the phase of the gap. Others have been designed specifically to probe this phase,[3–7] but not all give the same results and some controversy remains. The optical conductivity is not a phase sensitive quantity so we expect that a simple model in which the gap has an angular dependence on the two-dimensional Fermi surface of the form $\cos(2\theta)$, to be representative of any case for which the gap has zeros on the Fermi surface.

On the theoretical side, there now exists a large literature[16–34] on d-wave superconductivity. These works extend some of the previous calculations of superconducting properties performed for a p-wave gap,[35–39] which were motivated primarily by experiments on the heavy fermion superconductors. Much of the d-wave literature is general and is quite independent of the mechanism that leads to such a gap. One of many possibilities for mechanism is the nearly antiferromagnetic Fermi liquid[20–25] in which the pairing is envisaged to be due to the exchange of antiferromagnetic spin fluctuations. We have nothing new to say about this possibility here. Rather we will simply assume d-wave symmetry for the pairing interaction which is taken to be separable in initial and final momentum and then proceed to the calculation of the conductivity. We will present results for the infrared conductivity in a formalism which includes inelastic scattering through an electron-boson spectral density. This spectral density is also assumed to cause the superconductivity. In addition, impurity scattering will be treated in the unitary limit (strong scattering) and in Born approximation (weak scattering).[40] It is now well established that Zn and Ni in YBa$_2$Cu$_3$O$_{6.95}$ (YBCO) can have very different effects on superconducting properties.[41–44] As an example, Ni in small concentrations does not change the power law observed for the low temperature dependence of the penetration depth, while additions of Zn changes it from T to a T^2 law. This is what is expected for resonant scattering in the unitary limit.[37] Thus Ni may be in the Born limit (weak scattering) while Zn is in the opposite limit, namely the unitary limit.

The formalism employed involves generalized[44] Eliashberg equations in which the interaction kernel is taken to be a product of two separate functions of momentum and frequency and as a further simplification, a separable model is used for the angular dependence of the pairing. These assumptions lead to a gap which is proportional to $\cos(2\theta)$ where θ is an angle along the cylindrical Fermi surface in the two-dimensional CuO$_2$ planar Brillouin zone. The frequency dependence of the pairing interaction is accounted for, in the usual way, through an electron-boson spectral density $\alpha^2F(\omega)$. The form of this function is not our primary interest here and will be modeled. It is fixed for a spin function mechanism throughout the calculation. Impurity scattering enters as an extra term in both of the generalized Eliashberg equations for the gap and renormalization function. The form of the impurity term is different depending on resonant or Born scattering, but the general structure of the equations is not. The two coupled nonlinear Eliashberg equations must be solved numerically by successive iteration for each impurity concentration. From the solution of these equations on the real frequency axis, the conductivity is computed from an

appropriate Kubo formula for the current-current correlation function. The ratio of the real to imaginary part of the conductivity is used to define an inelastic scattering rate as a function of frequency which is compared with experimental results.

In Sec. II, we present the necessary formalism. Numerical results are found in Sec. III and a brief conclusion in Sec. IV.

II. FORMALISM

In Nambu notation, the conductivity at frequency v, which is denoted by $\sigma(v)$, can be written in terms of the 2×2 matrix Green's function $G_s(\mathbf{p}, \omega)$ in the superconducting state with $\mathbf{p}$ momentum and ω energy. The expression for $\sigma(v)$, the in-plane conductivity, is[45–52]

$$\sigma(v) = \frac{i}{v} \frac{2e^2 v_F^2 N(0)}{3} \left\langle \text{tr}\left\{ \int d\epsilon_{\mathbf{p}} \int d\Omega \, f(\Omega)\left(-\frac{1}{\pi} \right) \text{Im} G_s(\mathbf{p}, \Omega + i0^+)[G_s(\mathbf{p}, \Omega + v + i0^+) + G_s(\mathbf{p}, \Omega - v - i0^+)] \right\} \right\rangle, \quad (1)$$

where tr denotes the trace and the brackets $\langle \rangle$ indicate an average over the angles θ on the Fermi surface. The Fermi velocity is v_F, e is the charge on the electron, $N(0)$ is the electronic density of states taken out of the energy integral and pinned to its value at the Fermi surface, and $f(\Omega)$ is the Fermi Dirac thermal distribution. The integration over energy $\epsilon_{\mathbf{p}}$ in Eq. (1) can be carried out and, after considerable algebra, we arrive at a formula for $\sigma(v)$ of the form

$$\sigma(v) = \frac{i}{v} \frac{e^2 N(0) v_F^2}{3} \left\langle \int_0^\infty d\Omega \tanh\left(\frac{\Omega}{2T} \right) \frac{1}{E(\Omega; \theta) + E(\Omega + v; \theta)} [1 - N(\Omega; \theta)N(\Omega + v; \theta) - P(\Omega; \theta)P(\Omega + v; \theta)] \right.$$

$$+ \int_0^\infty d\Omega \tanh\left(\frac{\Omega + v}{2T} \right) \frac{1}{E^*(\Omega; \theta) + E^*(\Omega + v; \theta)} [1 - N^*(\Omega; \theta)N^*(\Omega + v; \theta) - P^*(\Omega; \theta)P^*(\Omega + v; \theta)]$$

$$+ \int_0^\infty d\Omega \left[\tanh\left(\frac{\Omega + v}{2T} \right) - \tanh\left(\frac{\Omega}{2T} \right) \right] \frac{1}{E(\Omega + v; \theta) - E^*(\Omega; \theta)} [1 + N^*(\Omega; \theta)N(\Omega + v; \theta) + P^*(\Omega; \theta)P(\Omega + v; \theta)]$$

$$+ \int_{-v}^0 d\Omega \tanh\left(\frac{\Omega + v}{2T} \right) \times \left[\frac{1}{E^*(\Omega; \theta) + E^*(\Omega + v; \theta)} [1 - N^*(\Omega; \theta)N^*(\Omega + v; \theta) - P^*(\Omega; \theta)P^*(\Omega + v; \theta)] \right.$$

$$\left. \left. + \frac{1}{E(\Omega + v; \theta) - E^*(\Omega; \theta)} [1 + N^*(\Omega; \theta)N(\Omega + v; \theta) + P^*(\Omega; \theta)P(\Omega + v; \theta)] \right] \right\rangle, \quad (2)$$

with

$$E(\omega; \theta) = \sqrt{\widetilde{\omega}_{\mathbf{p}}^2(\omega) - \widetilde{\Delta}_{\mathbf{p}}^2(\omega)} \qquad (3)$$

and

$$N(\omega; \theta) = \frac{\widetilde{\omega}_{\mathbf{p}}^2(\omega)}{E(\omega; \theta)}, \quad P(\omega) = \frac{\widetilde{\Delta}_{\mathbf{p}}^2(\omega)}{E(\omega; \theta)}; \qquad (4)$$

in the above, the star refers to the complex conjugate. Here, $\widetilde{\omega}_{\mathbf{p}}(\omega) \equiv \widetilde{\omega}(\omega; \theta)$ and $\widetilde{\Delta}_{\mathbf{p}}(\omega) \equiv \widetilde{\Delta}(\omega; \theta)$ are the renormalization and pairing function, respectively, taken on the real frequency axis and written for an anisotropic state. They are solutions of the real frequency axis Eliashberg equations. First, these equations need to be written on the imaginary Matsurbara frequency axis with $i\omega_n \equiv i(2n+1)\pi T$ with T the temperature. For a separable pairing potential for scattering from $\mathbf{k}$ to $\mathbf{k}'$ at the Fermi surface, which is attractive, and of the form $g \cos(2\theta)\lambda(n-m)\cos(2\theta')$ (Ref. 44) in the pairing channel and, for simplicity, assumed to be isotropic and equal to $\lambda(n-m)$ in the renormalization channel, they are

$$\widetilde{\Delta}(i\omega_n; \theta) = \pi T g \sum_m \cos(2\theta)\lambda(m-n)$$

$$\times \left\langle \frac{\cos(2\theta')\widetilde{\Delta}(i\omega_m; \theta')}{\sqrt{\widetilde{\omega}(i\omega_m)^2 + \widetilde{\Delta}(i\omega_m; \theta')^2}} \right\rangle' \quad (5a)$$

and

$$\widetilde{\omega}(i\omega_n) = \omega_n + \pi T \sum_m \lambda(m-n)$$

$$\times \left\langle \frac{\widetilde{\omega}(i\omega_m)}{\sqrt{\widetilde{\omega}(i\omega_m)^2 + \widetilde{\Delta}(i\omega_m; \theta')^2}} \right\rangle', \quad (5b)$$

where g is a measure of the d- to s-wave admixture in the interaction. The numerical results, to be presented in the next section, do not depend critically on the value of g. Here we will present results only for $g = 0.8$ although we have carried out calculations for other values. The quantity $\lambda(m-n)$ has the usual form

$$\lambda(n-m) = \int \frac{2\Omega \alpha^2 F(\Omega) d\Omega}{\Omega^2 + (\omega_n - \omega_m)^2}, \qquad (6)$$

where $\alpha^2 F(\Omega)$ is the electron boson spectral density involved in the interaction. Its precise value will depend on mechanism. Here, for convenience, we will take it to have the shape of the spectral density derived from the antiferromagnetic spin susceptibility rather than from phonons.[53,54] In as much as this choice is not critical to the numerical results obtained, we are not committing ourselves exclusively to an underlying spin fluctuation mechanism involving antiferromagnetic paramagnons. The form of $\alpha^2 F(\Omega)$ chosen is a constant times $(\omega/\omega_{SF})/[1+(\omega/\omega_{SF})^2]$ with the paramagnon frequency $\omega_{SF} \cong 30.0$ meV.[54] The ratio of T_c/ω_{SF} is the relevant strong coupling index.[54] The absolute strength of the spectral density in (6) is, of course, what determines the size of T_c which we can think of as typically 100 K for the high-T_c oxides. It also causes the inelastic scattering which in our work corresponds to a rate of order T_c at the critical temperature.

As written, Eqs. 5(a) and 5(b) do not depend on impurity scattering. To include this possibility, we need to add onto the right-hand side of 5(b) a term of the form

$$\pi \Gamma^+ \frac{\langle \Omega(i\omega_n;\theta) \rangle}{c^2 + \langle \Omega(i\omega_n;\theta) \rangle^2 + \langle D(i\omega_n;\theta) \rangle^2}, \qquad (7)$$

where Γ^+ is proportional to the impurity concentration and c is related to the electron phase shift for scattering off the impurity. For unitary scattering, it is equal to zero while $c \to \infty$ gives the Born approximation. The actual value of Γ^+ will not be specified here. As impurities are added to a d-wave superconductor, the value of T_c is reduced below its pure case magnitude (T_{c0}) and the ratio of T_c to T_{c0} will be used as an index of impurity scattering instead of Γ^+. To complete the specification of (7), we have

$$D(i\omega_n;\theta) \equiv \frac{\widetilde{\Delta}(i\omega_n;\theta)}{\sqrt{\widetilde{\omega}(i\omega_n)^2 + \widetilde{\Delta}(i\omega_n;\theta)^2}} \qquad (8a)$$

and

$$\Omega(i\omega_n;\theta) = \frac{\widetilde{\omega}(i\omega_n)}{\sqrt{\widetilde{\omega}(i\omega_n)^2 + \widetilde{\Delta}(i\omega_n;\theta)^2}}. \qquad (8b)$$

Note that the average $\langle D(i\omega_n;\theta) \rangle$ of Eq. (7) will exactly vanish for pure d-wave symmetry as we have assumed here.

While certain quantities, such as the penetration depth, can be obtained quite directly from the numerical solution on the imaginary frequency axis, i.e., from $\widetilde{\Delta}(i\omega_n;\theta)$ and $\widetilde{\omega}(i\omega_n)$, the real frequency axis solutions are needed for the calculation of the conductivity. The real frequency axis equations for $\widetilde{\Delta}(\omega+i\delta;\theta)$ and $\widetilde{\omega}(\omega+i\delta)$ with δ infinitesimal are much more complicated than Eqs. (5a) and (5b). They can be written in the form[44,55]

$$\widetilde{\Delta}(\omega+i\delta;\theta)$$
$$= i\pi Tg \sum_{m=0} \cos(2\theta)[\lambda(\omega-i\omega_m)+\lambda(\omega+i\omega_m)]$$

$$\times \left\langle \frac{\cos(2\theta')\widetilde{\Delta}(i\omega_m;\theta')}{\sqrt{\widetilde{\omega}(i\omega_m)^2+\widetilde{\Delta}(i\omega_m;\theta')^2}} \right\rangle'$$

$$+ i\pi \int_{-\infty}^{+\infty} dz \cos(2\theta)\alpha^2 F(z)[n(z)+f(z-\omega)]$$

$$\times \left\langle \frac{\cos(2\theta')\widetilde{\Delta}(\omega-z+i\delta;\theta')}{\sqrt{\widetilde{\omega}(\omega-z+i\delta)^2-\widetilde{\Delta}(\omega-z+i\delta;\theta')^2}} \right\rangle' \qquad (9a)$$

and

$$\widetilde{\omega}(\omega+i\delta) = \omega + i\pi T \sum_{m=0}^{\infty} [\lambda(\omega-i\omega_m)-\lambda(\omega+i\omega_m)]$$

$$\times \left\langle \frac{\widetilde{\omega}(i\omega_m)}{\sqrt{\widetilde{\omega}(i\omega_m)^2+\widetilde{\Delta}(i\omega_m;\theta')^2}} \right\rangle'$$

$$+ i\pi \int_{-\infty}^{+\infty} dz \, \alpha^2 F(z)[n(z)+f(z-\omega)]$$

$$\times \left\langle \frac{\widetilde{\omega}(\omega-z+i\delta)}{\sqrt{\widetilde{\omega}(\omega-z+i\delta)^2-\widetilde{\Delta}(\omega-z+i\delta;\theta')^2}} \right\rangle'$$

$$+ i\pi\Gamma^+ \frac{\Omega(\omega)}{c^2 + D^2(\omega) + \Omega^2(\omega)}, \qquad (9b)$$

where

$$\lambda(\omega) = \int_{-\infty}^{+\infty} \frac{\alpha^2 F(\Omega)d\Omega}{\omega-\Omega+i0^+}, \qquad (10)$$

$$D(\omega) = \left\langle \frac{\widetilde{\Delta}(\omega+i\delta;\theta)}{\sqrt{\widetilde{\omega}(\omega+i\delta)^2-\widetilde{\Delta}(\omega+i\delta;\theta)^2}} \right\rangle, \qquad (11)$$

and

$$\Omega(\omega) = \left\langle \frac{\widetilde{\omega}(\omega+i\delta)}{\sqrt{\widetilde{\omega}(\omega+i\delta)^2-\widetilde{\Delta}(\omega+i\delta;\theta)^2}} \right\rangle. \qquad (12)$$

In Eqs. (9a) and (9b), $n(z)$ and $f(z)$ are, respectively, the Bose-Einstein and Fermi-Dirac distribution functions at temperature T. We note that in our simplified model for the momentum dependence of the interaction, the renormalized Matsubara frequency $\widetilde{\omega}(\omega+i0^+)$ does not itself depend on angles. In principle, we could also have taken a different form for $\lambda(n-m)$ in the two channels of Eqs. (5a) and (5b) but this would introduce a new uncontrolled function into the theory, which we want to avoid, and only g is introduced with the same form of $\alpha^2 F(\Omega)$.

III. NUMERICAL RESULTS

As we will be mainly interested in a comparison of our results for resonant impurity scattering (strong scattering) with similar results for Born scattering (weak scattering) and do not want to commit ourselves to a particular value of the plasma frequency, we will present results for the conductivity in arbitrary units. What is left out of our computer programs is the factor $2/3 \ e^2 v_F^2 N(0)$ in formula (1). To get the actual conductivity, it is therefore necessary to multiply the results presented by $ne^2/2m$ where n is the electron density and m the electron mass. Also, all our results in the superconducting state will be given with reference to reduced sample temperature T/T_c where T_c is the critical temperature of the sample which can contain impurities. In a d-wave superconductor, adding impurities, of course, leads to a reduction in critical temperature.

Results for the real part of the conductivity have already been discussed by Carbotte, Jiang, Basov, and Timusk[40] although the amount of inelastic scattering included in their work was considerably less than the amount included here. They also employed a Pb spectrum to model the boson spectral density $\alpha^2F(\Omega)$ and the coupling strength, as measured by the strong coupling parameter $T_c/\omega_{\log}$,[53,54] was set equal to 0.1 where $\omega_{\log}$ is the characteristic boson energy involved. Here we use instead a form for $\alpha^2F(\Omega)$ which may be more appropriate to a spin fluctuation spectrum, namely

$$\alpha^2F(\Omega) = h\left(\frac{(\omega/\omega_{SF})}{1+(\omega/\omega_{SF})^2} \right), \qquad (13)$$

with h chosen to get critical temperature value T_c of 100 K for the pure case (no impurities). This is typical for the oxides. The other parameter, which fixes the boson energy scale, ω_{SF}, was set equal to 30 meV so that the strong coupling parameter $T_c/\omega_{\log}$ is now equal to 0.31. Different choices of this spectrum could be made particularly if one wished to model some other known and definite mechanism. In particular, models that include enhanced low frequency scattering, discussed below. Here we will stay with the choice (13) as the actual mechanism causing the superconductivity in the oxides is not yet known.

In Fig. 1(a), we show our results for the real part of the conductivity in the superconducting state $\sigma_1^S(\Omega)$ as a function of frequency Ω in meV for the clean limit, i.e., $\Gamma^+=0$ in Eqs. (7) and (9). In this limit, inelastic scattering remains, and at any finite temperature, there will be a finite scattering rate dependent on he assumed spectral density $\alpha^2F(\Omega)$ of Eq. (13). In out numerical work, we have taken $g=0.8$ in Eqs. (5a) and (9a) and numerical results are presented for five values of temperature, namely $T=0.995T_c$ (very near T_c) (solid line), $T=0.9T_c$ (dotted line), $T=0.7T_c$ (short dashed line), $T=0.5T_c$ (long dashed line), and $T=0.1T_c$ (short dashed-dotted line). On comparison with the results presented in Ref. 40, the solid curve very near T_c now does not show a region of depressed conductivity between the low frequency Drude peak and the boson assisted absorption region at higher energies, a feature that is in accord with the experimental data. The boson assisted process, of course, remains even at zero temperature and is seen clearly in our results for $T=0.1T_c$ (short dashed-dotted curve) in which
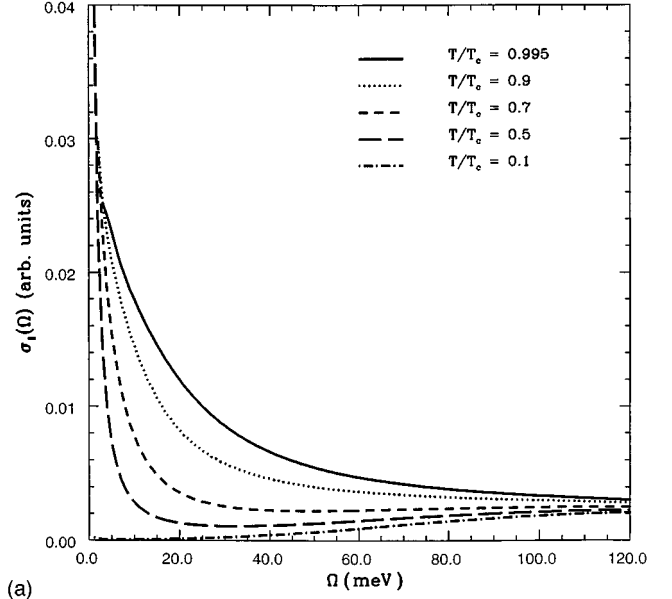
(a)
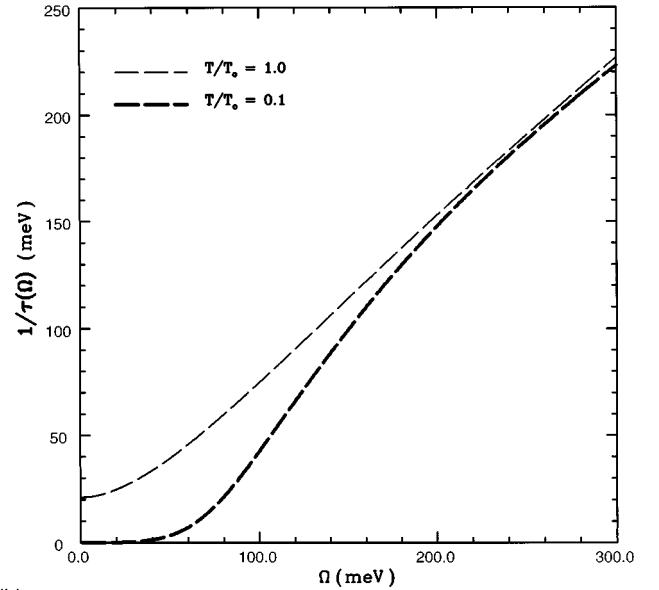
(b)

FIG. 1. (a) The real part of the superconducting state conductivity $\sigma_1^s(\Omega)$ in arbitrary units as a function of frequency Ω in meV. The five temperature values are $T=0.995T_c$ (solid curve) very near the critical temperature, $T=0.9T_c$ (dotted curve), $T=0.7T_c$ (short dashed curve), $T=0.5T_c$ (long dashed curve), and $T=0.1T_c$ (short dashed-dotted curve). (b) gives the scattering rate $1/\tau(\Omega)$ in meV vs Ω in meV derived from our conductivity data as defined in Eq. (14), namely $\Omega\sigma_1^s(\Omega)/\sigma_2^s(\Omega)$. Light long dashed line is for $T=T_c$ (normal state) and dark long dashed for $T=0.1T_c$ (superconducting state).

case the low frequency Drude peak is so narrow that it does not show explicitly. On the other hand, for the long dashed curve with $T=0.5T_c$, one can see a slight dip between these two regions with the conductivity smaller in magnitude around 30–40 meV than it is for larger or smaller frequencies. The reason for this difference with previous results is that, here, we have included a more realistic amount of inelastic scattering. In terms of the coupling strength param-

eters $T_c/\omega_{\log}$, where $\omega_{\log}$ is the characteristic boson frequency in the model for $\alpha^2 F(\Omega)$, it has gone to 0.31 from 0.1. One characterization of the amount of inelastic scattering present is to form the ratio

$$\frac{\Omega \sigma_1^s(\Omega)}{\sigma_2^s(\Omega)} \equiv \frac{1}{\tau(\Omega)}, \qquad (14)$$

which we will denote by $1/\tau(\Omega)$. In Eq. (14), both real $\sigma_1^s(\Omega)$ and imaginary part $\sigma_2^s(\Omega)$ are taken in the superconducting state. As defined by Eq. (14), $1/\tau(\Omega)$ has units of energy and would reduce to the impurity scattering rate in a simple Drude model of the normal state. The form given by Eq. (14) has its origin in the extended or generalized Drude form written as

$$\sigma(\Omega) = \frac{ne^2}{m(\Omega)} \left[\frac{1}{\frac{1}{\tau(\Omega)} - i\Omega} \right], \qquad (15)$$

where $m(\Omega)/m$ is a frequency dependent mass renormalization factor given by

$$\frac{m(\Omega)}{m} = \frac{ne^2}{m} \frac{\frac{\sigma_2(\Omega)}{\omega}}{\sigma_1(\Omega)^2 + \sigma_2(\Omega)^2} \qquad (16)$$

and $\tau(\Omega)$ is given by formula (14). The forms (15) and (16) are a general representation of any complex function $\sigma(\Omega)$ but $\tau^{-1}(\Omega)$ so defined, while equal to the impurity scattering rate in the Drude model, is not easily related to the inelastic quasiparticle scattering rate for a coupled electron-boson system. This is true even in the normal state as discussed by Dolgov, Maksimov, and Shulga.[51] Nevertheless, we will use (14) even in the superconducting state as some characteristic scattering rate.

Results for the pure case (no impurity scattering) are shown in Fig. 1(b) for two temperatures, namely $T = T_c$ (light long dashed curve) in the normal state and $T = 0.1 T_c$ (dark long dashed curve). What is plotted is the ratio (14) for the rate $1/\tau(\Omega)$ in meV as a function of energy Ω in meV. Note that over a considerable range at the higher frequencies, the curves nearly, but not perfectly, linear. The variation with Ω, in this region, could be changed with a different form of the assumed spectrum (13), but this will not be done here since we are only interested in a qualitative comparison with experiments, and we do not want to do any fitting. In Fig. 2, we show our experimental results for the scattering rate (14) $1/\tau_a(\Omega)$ in $(cm)^{-1}$ as a function of wave number in (cm^{-1}) up to 2000 cm^{-1} for the case of twinned, high quality crystals of $YBa_2Cu_3O_{6.95}$ with electric field in the CuO_2 plane of the sample oriented along the a axis. At high frequencies, in the normal state at a temperature just above the critical temperature (T_c), the scattering rate $1/\tau(\Omega)$ exhibits a quasilinear behavior over a wide range of frequency and its slope, in dimensionless units, is approximately 0.75 in both theory and experiment. From this good agreement, we conclude that our theoretical approach, which is based on a Fermi liquid (FL) picture, is well able to describe the absolute magnitude and frequency dependence of the observed inelastic scattering in this region. As the frequency Ω is re-
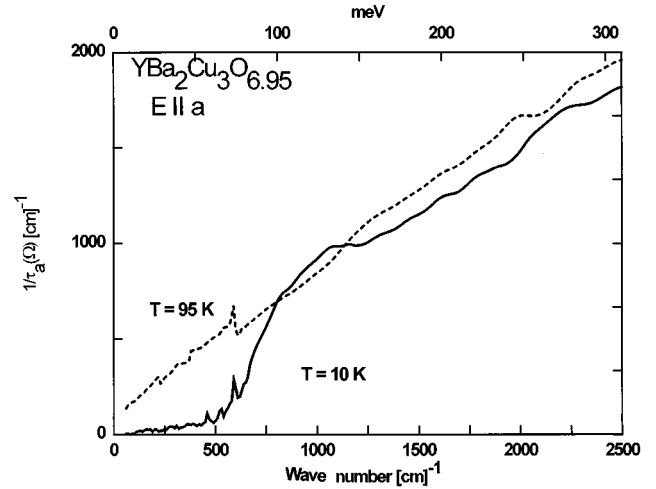
FIG. 2. Our experimental results for the frequency dependence (Ω) of the scattering rate $1/\tau(\Omega)$ in cm^{-1} as a function of wave number in cm^{-1} for $YBa_2Cu_3O_{6.95}$. A pure high quality sample was used and the results are for the in plane a or b axis at temperature $T = 10$ K.

duced towards zero, however, theory and experiment begin to deviate. While both show a positive intercept at $\Omega = 0$, which is somewhat smaller in the data than in the theory (~ 20 meV), the quasilinear behavior is found to persist all the way to $\Omega = 0$ in the data. By contrast, a saturating behavior, characteristic of a Fermi liquid approach, is seen in the theoretical curve. This may indicate a breakdown of FL theory in optimally doped samples.

Turning next to the superconducting state, both theory and experiment fall a little below the $T = T_c$ normal state curve at high frequency. At lower frequencies, the suppression in the superconducting state increasing rapidly with decreasing frequency and $1/\tau(\Omega)$ is very small below 50 meV in both theory and experiment. Theory, however, predicts smooth behavior for the suppression in the superconducting state on an energy scale of about 110 meV in frequency Ω, while the data indicates some threshold behavior centered around $\Omega = 90$ meV. This sharp drop could be simulated in our theory if a different spectrum was used instead of (13). Also, it may well be that the spectrum $\alpha^2 F(\Omega)$ is different in superconducting and normal state so that a reasonable fit to both normal and superconducting state could be achieved this way. Changing the shape of the assumed spectrum (13), to gain better agreement with experimental data on $1/\tau(\Omega)$, however, is not our aim here. Achieving such a fit could be misleading and obscure the need for a different explanation. What is important is that the amount of inelastic scattering included in our work is of the same order of magnitude as is observed and that the overall predicted frequency dependence of $1/\tau(\Omega)$ is also in reasonable agreement with experiment. At lower frequencies, however, we have noted some important qualitative differences which could, at least partially, be accounted for through appropriate changes in the boson spectrum (13). We have chosen not to do this, however, because the differences could also be due to a breakdown of the Fermi liquid approach used in this work.
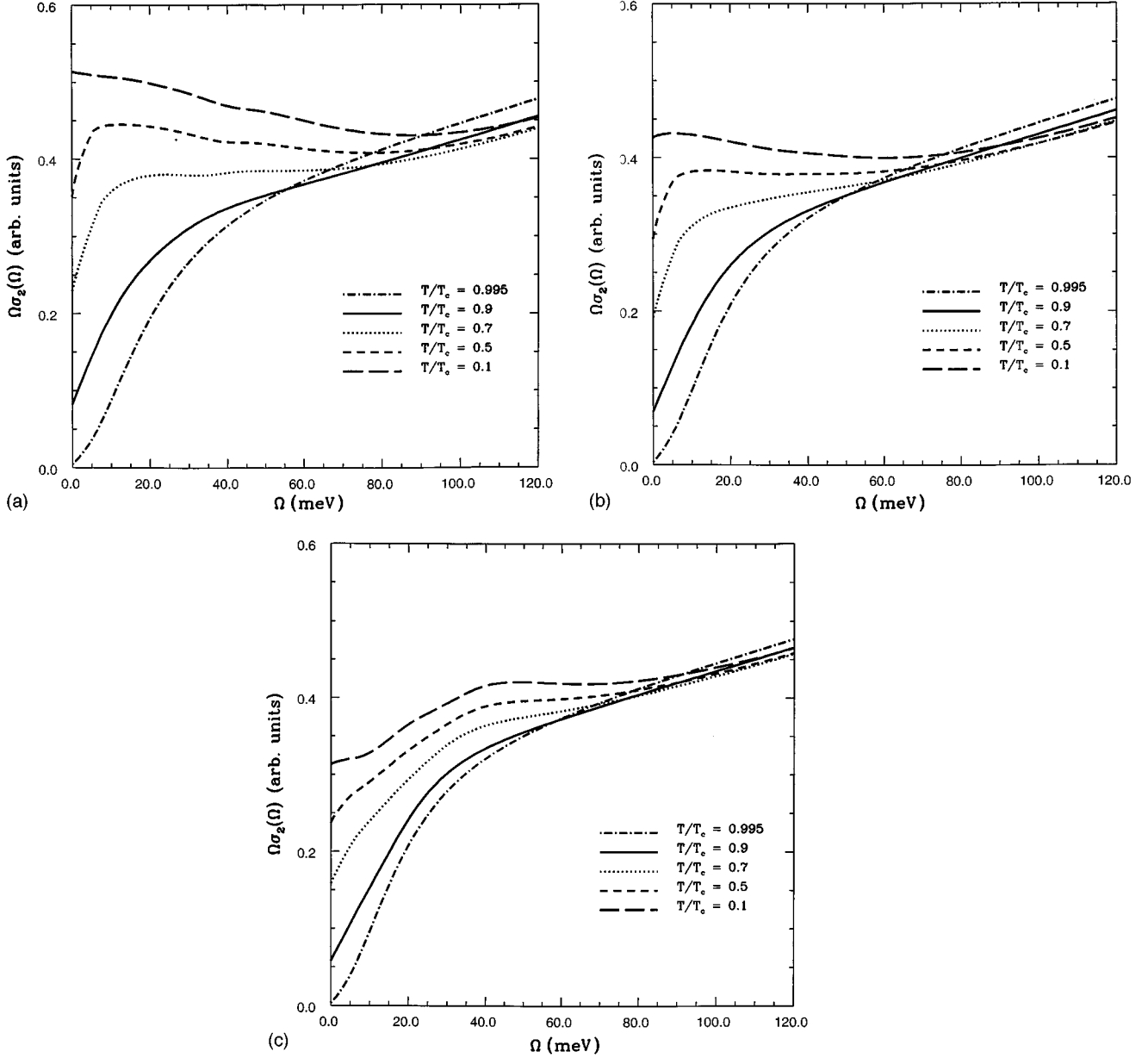
FIG. 3. The product of frequency Ω times the imaginary part of the infrared conductivity $\sigma_2^s(\Omega)$ in the superconducting state as a function of frequency Ω in meV. Results for five temperatures are shown, namely $T = 0.995 T_c$ (short dashed-dotted curve), $T = 0.9 T_c$ (solid curve), $T = 0.7 T_c$ (dotted curve), $T = 0.5 T_c$ (short dashed curve), and $T = 0.1 T_c$ (long dashed curve). The zero frequency limit of $\Omega \sigma_2^s(\Omega)$ gives the inverse of the square of the penetration depth in the London limit according to Eq. (15). The units on the conductivity are $ne^2/2m$ and frame (a) is for the pure case with pure crystal critical temperature value of $T_c = 100$ K. Frames (b) and (c) apply respectively to an impure case with T_c reduced to 80 K by the elastic scattering due to impurities in Born (weak scattering), limit and unitary (strong scattering), respectively.

In Fig. 3, we show our theoretical results for the imaginary part of the conductivity. Instead of presenting $\sigma_2(\Omega)$, it is convenient to multiply first by a factor of frequency ω (real energy in meV in our case). One reason for making such plots is that the penetration depth $\lambda(\omega)$ is related to $\omega \sigma_2^s(\omega)$ through

$$\frac{1}{\lambda^2(\Omega)} = \frac{4\pi}{c^2} \Omega \sigma_2^s(\Omega) \qquad (17)$$

and the London penetration depth λ_L is the zero frequency limit of (15). Here c is the velocity of light.

Figure 3(a) gives our results for the pure case, i.e., no impurity scattering included in the generalized Eliashberg equations (5) and (9). Of course, inelastic scattering remains. The top curve is for $T = 0.1 T_c$ (long dashed line), the second for $T = 0.5 T_C$ (short dashed line), the next for $T = 0.7 T_c$ (dotted line), the second lowest for $T = 0.9 T_c$ (solid line), and the lowest for $T = 0.995 T_c$ (short dashed dotted line) which is almost at the critical temperature T_c. The first thing to be noted is that the zero frequency limit of these curves is proportional to the inverse square of the penetration depth. To obtain Fig. 3(a), we have solved numerically the real frequency form of the Eliashberg equations given in formulas

(9a) and (9b) and used these solutions in Eq. (2) for the conductivity. For the penetration depth, however, a much simpler procedure is to use the imaginary frequency solutions and the Matsubara representation form for the London penetration depth, namely

$$\frac{1}{\lambda_L^2(T)} \propto \left\langle \pi T \sum_m \frac{\widetilde{\Delta}^2(i\omega_m;\theta)}{[\widetilde{\omega}^2(i\omega_m) + \widetilde{\Delta}^2(i\omega_m;\theta)]^{3/2}} \right\rangle, \quad (18)$$

which serves as a check on our numerical evaluation using a real frequency axis formalism. It is quite clear from the figure that optical experiments would need to be carried out at rather low values of frequency if one wishes to get accurate values of the penetration depth from this method because $\Omega\sigma_2^s(\Omega)$ is seen to be a rapidly varying function of Ω in the relevant region. Note that multiplication of the results of Fig. 3 by $ne^2/2m$, as is also the case for the real part of the conductivity $\sigma_1^s(\Omega)$ in Fig. 1, will restore units but a choice of the plasma frequency is still needed to compare with experimental quantities. This is not the case for the scattering times presented in Fig. 2 which are independent of plasma frequency and are in units of energy.

We note that the largest changes in $\Omega\sigma_2^s(\Omega)$ as the temperature is changed occurs for low frequencies below roughly 40 meV which is between 4 to 5 times T_c. The last curve shown in Fig. 3(a), which applies for a temperature very close to T_c, almost reaches zero at $\Omega \to 0$. In this case, the conductivity $\Omega\sigma_2(\Omega)$ is not very different from its normal state value at $T = T_c = 100$ K. However, because we have included inelastic scattering in our calculated results through the spectral density (13), the normal state results for $\Omega\sigma_2^s(\Omega)$ do not reduce to a simple Drude of the form

$$\frac{ne^2}{m} \frac{(\Omega\tau)^2}{1+(\Omega\tau)^2}, \quad (19)$$

with τ some scattering time which would hold for all frequencies. This was discussed in the work of Marsiglio, Carbotte, Puchkov, and Timusk.[56] These authors have found that only the low frequency part of the curve for $\Omega\sigma_2^s(\Omega)$ at T_c fits the Drude from (19) with m and τ in Eq. (17) replaced by a renormalized mass m^* and τ^* with each of these two quantities having a very specific form which is given in Ref. 56 but which applies only in a very narrow energy region near $\Omega = 0$ and fails outside this region. What we are saying is that the inelastic scattering, even in the normal state, profoundly changes the shape of the imaginary part of the conductivity and no Drude form with constant m and τ will fit the theoretical results over an extended frequency range. Of course, the extended Drude form of formula (15) will always produce a fit.

Figures 3(b) and 3(c) include impurities and apply respectively to Born scattering, i.e., the limit $c \to \infty$ in Eqs. (7) and (9) and unitary scattering $c \to 0$, respectively. The temperature values are the same as for Fig. 3(a). On examination of the figures, it is clear that the curves for $\Omega\sigma_2^s(\Omega)$ vs Ω are least affected by the introduction of impurity scattering in the high energy region near 120 meV. At low frequencies, the curves are strongly reduced over the corresponding pure case by the introduction of impurity scattering rate which is equal to 3.252 meV. This is the value needed to reduce the critical
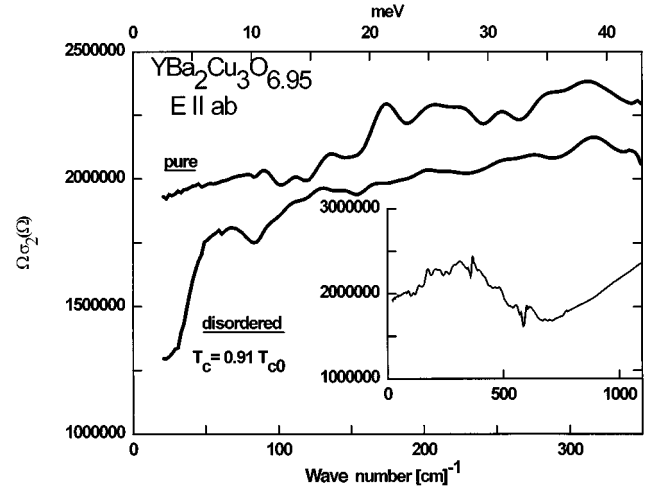
FIG. 4. Experimental results for the product of the frequency Ω times the imaginary part of the conductivity $\sigma_2^s(\Omega)$ in the superconducting state at $T = 10$ K for a YBa$_2$Cu$_3$O$_{6.95}$ pure high quality crystal as a function of wave number Ω in cm^{-1}. The upper curve is for the pure case and the lower case after crystal irradiation with $T_c = 0.91 T_{c0}$. The inset shows a larger frequency range.

temperature from 100 to 80 K, i.e., by 20% of its pure value, and increase the penetration depth.

The penetration depth increases with increasing impurity content in analogy to ordinary s-wave BCS theory where the penetration depth $\lambda_l(0)$, at zero temperature, for a sample with a finite mean free path (l), is related to its clean value (λ_∞) with $l = \infty$ (infinite mean free path) by

$$\lambda_l = \lambda_\infty \sqrt{1+\xi/l}, \quad (20)$$

where ξ is the superconducting coherence length.

In Fig. 4, we show experimental results for $\Omega\sigma_2^s(\Omega)$ vs Ω for a single crystal high purity sample of YBa$_2$Cu$_3$O$_{6.95}$ at reduced temperature $T/T_c = 0.1$. The upper solid curve has a T_{c0} value of 93.5 K, whereas the lower curve was obtained with the same crystal after it was damaged by irradiation with low energy He ions.[57] The critical temperature of the disordered material was suppressed down to a value equal to $0.91 T_{c0}$. It is clear from the plot that $\Omega\sigma_2^s(\Omega)$ is significantly affected by disorder in the entire range shown up to $\Omega \leq 350$ cm^{-1} and that the qualitative behavior predicted in Fig. 3 (long dashed curves) is confirmed in the experiments. Note that in our theoretical curve, the critical temperature of the impure samples is $0.8 T_{c0}$, while in the experiments, it is only $0.91 T_{c0}$. We also note that the low frequency limit of our experimental results coincides with our estimate of the penetration depth made from the sum rule analysis of the real part of $\sigma_1^s(\Omega)$.[59] Also, infrared experiments carried out on YBCO 124 crystals doped with Zn show the same tendency.[58] We point out that the general behavior of $\Omega\sigma_2^s(\Omega)$ vs Ω shown in a larger energy scale in the inset of Fig. 4 is also in qualitative accord with our theoretical results. More importantly, however, is the smooth behavior predicted and observed for $\Omega\sigma_2^s(\Omega)$ vs Ω in the region of twice the gap value. This is in sharp contrast to the case of an s-wave superconductor with impurities (but not necessarily

phonon mediated), for which Marsiglio, Carbotte, Puchkov, and Timusk[56] have found that a prominent distinct dip is expected in $\Omega\sigma_2^s(\Omega)$ vs Ω at twice the gap value. While this structure is modified somewhat with increasing impurity content, it remains distinct and prominent and can be easily used to identify a gap value. This has been observed in the case of BaKBiO (Refs. 57–60) and leaves little doubt that this material is an s-save superconductor although Marsiglio, Carbotte, Puchkov, and Timusk[56] conclude that the amount of inelastic scattering observed in this material (from a study of the temperature dependence of the width of the Drude peak) is too weak for it to be a conventional electron-phonon superconductor. By contrast, for $YBa_2Cu_3O_{6.95}$, the results presented in Fig. 4 show smooth behavior with no gap structure as predicted for a d-wave superconductor with impurities and shown in our Fig. 3. There can be little doubt that $YBa_2Cu_3O_{6.95}$ is not isotropic s-wave and that the observed behavior of $\Omega\sigma_2^s(\Omega)$ vs Ω is consistent with d-wave. It should be pointed out, however, in making this identification, that the imaginary part of the conductivity is a quantity that is only sensitive to the nodes in the gap and not to its phase and so falls in the same category as the thermodynamics, the penetration depth, the angular resolved photo emission, etc.

IV. SUMMARY AND CONCLUSION

Within a generalized Eliashberg formalism, which includes an angular dependence of the gap of the form $\cos(2\theta)$ with θ an angle over the Fermi circle in the two-dimensional Brillouin zone of copper oxygen plane, we have computed the conductivity in the infrared region including impurities in Born and in the resonant scattering limit (unitary). In our formalism, the electron boson spectral density appearing in the set of two coupled nonlinear Eliashberg equations for the gap and renormalization factor determines the inelastic scattering as well as describes the pairing mechanism. A form was chosen for this function which was motivated by a spin fluctuation mechanism but the results obtained for σ are not entirely specific to this case and should illustrate the effect of large amounts of inelastic scattering in general.

We have given results for the real part of the conductivity as a function of frequency for the pure case when the amount of inelastic scattering at T_c is of the order of T_c. The results are further analyzed in terms of frequency dependent scattering rate $1/\tau(\Omega)$ defined as $\Omega\sigma_1^s(\Omega)/\sigma_2^s(\Omega)$ and when compared with our experimental results are found to be in qualitative agreement with the data on pure high quality twinned crystals of $YBa_2Cu_3O_{6.95}$ as to order of magnitude of the scattering and its high frequency dependence. Differences between theory and experiment at low frequencies could be reduced with a different choice of electron-boson spectral density but may also find its explanation in the breakdown of the Fermi liquid approach used here.

Consideration of Ω times the imaginary part of the conductivity shows that finite frequency results can be used to safely obtain informtion on the impurity dependence of the penetration depth [which strictly depends on the limit $\Omega\sigma_2(\Omega)$, as Ω goes to zero] only if sufficiently small values of Ω are available. More importantly, the frequency dependence of this quantity in the gap region is found to be quite smooth and shows no dip in impure samples at twice the gap value (2Δ) in sharp contrast to the s-wave case. Experimentally, smooth behavior in qualitative agreement with our predictions is observed in disordered $YBa_2Cu_3O_{6.95}$ and $YBa_2Cu_4O_8$ while corresponding results in BaKBiO show the unmistakable characteristic sharp minimum at 2Δ which is expected for the isotropic s-wave case. Thus $\Omega\sigma_2(\Omega)$ vs Ω data in the infrared can be used to distinguish clearly between an s-wave superconductor with a definite gap and one with a distribution of gaps that go through zero on the Fermi surface. The method is only sensitive to the size of the gap and not to its phase, however.

ACKNOWLEDGMENTS

[1] T. Timusk and D. B. Tanner, in *Physical Properties of High Temperature Superconductors I*, edited by D. M. Ginsberg (World Scientific, Singapore, 1989), p. 339.

[2] D. B. Tanner and T. Timusk, in *Physical Properties of High Temperature Superconductors III*, edited by D. M. Ginsberg (World Scientific, Singapore, 1992).

[3] D. A. Wollman *et al.*, Phys. Rev. Lett. **71**, 2134 (1993).

[4] D. A. Brawner and H. R. Ott, Phys. Rev. B **50**, 6530 (1994).

[5] P. Chaudhari and S. Y. Lin, Phys. Rev. Lett. **72**, 1084 (1994).

[6] A. G. Sun *et al.*, Phys. Rev. Lett. **72**, 2267 (1994).

[7] C. C. Tsuei *et al.*, Phys. Rev. Lett. **73**, 539 (1994).

[8] W. N. Hardy *et al.*, Phys. Rev. Lett **70**, 3999 (1993).

[9] B. O. Wells *et al.*, Phys. Rev. **46**, 11 839 (1992).

[10] Z. X. Shen *et al.*, Phys. Rev. Lett. **70**, 1553 (1993).

[11] J. F. Annett and N. Goldenfeld, J. Low Temp. Phys. **89**, 197 (1992).

[12] R. J. Kelley, J. Ma, G. Margaritondo, and M. Onellion, Phys. Rev. Lett. **71**, 4051 (1993).

[13] D. S. Desseau *et al.*, Phys. Rev. Lett. **66**, 2160 (1991).

[14] H. Ding *et al.*, Phys. Rev. Lett. **50**, 1333 (1994).

[15] H. Ding. J. C. Campuzano, A. F. Bellman, T. Yokoya, M. R. Norman, M. Randeria, T. Takahasi, H. Katayama-Yoshida, T. Mochiku, K. Kadowaki, and G. Jennings, Phys. Rev. Lett. **74**, 2729 (1995).

[16] D. J. Scalapino, E. Loh, and J. E. Hirsch, Phys. Rev. B **34**, 8190 (1986).

[17] N. E. Bickers, R. T. Scalettar, and D. J. Scalapino, Int. J. Mod. Phys. B **1**, 687 (1987).

[18] A. J. Millis, S. Sachdev, and C. M. Varma, Phys. Rev. B **37**, 4975 (1988).

[19] K. Miyake, S. Schmitt-Rink, and C. M. Varma, Phys. Rev. B **34**, 6554 (1986).

[20] A. J. Millis, H. Monien, and D. Pines, Phys. Rev. B **42**, 167 (1990).

[21] P. Monthoux, A. V. Balatsky, and D. Pines, Phys. Rev. Lett. **67**, 3448 (1991).

[22] P. Monthoux and D. Pines, Phys Rev. B **47**, 6069 (1993).

[23] M. R. Norman, Phys. Rev. B **37**, 4987 (1988); **41**, 170 (1990).

[24] S. Wermbter and L. Tewordt, Phys. Rev. B **43**, 10 530 (1991).

[25] R. J. Radtke, S. Ullah, K. Levin, and M. R. Norman, Phys. Rev. B **46**, 11 975 (1992).

[26] St. Lenck and J. P. Carbotte, Phys. Rev. B **46**, 14 850 (1992).

[27] Q. Si, Y. Zha, K. Levin, and J. P. Lu, Phys. Rev. B **47**, 9055 (1993).

[28] P. Arberg, M. Mansor, and J. P. Carbotte, Solid State Commun. **86**, 671 (1993).

[29] E. J. Nicol, C. Jiang, and J. P. Carbotte, Phys. Rev. B **47**, 8131 (1993).

[30] E. Schachinger and J. P. Carbotte, Phys. Rev. B **43**, 10 279 (1991).

[31] M. Prohammer and J. P. Carbotte, Phys. Rev. B **43**, 5370 (1991).

[32] A. Perez-Gonzalez and J. P. Carbotte, Phys. Rev. B **45**, 9894 (1992).

[33] M. Prohammer and J. P. Carbotte, Phys. Rev. B **42**, 2032 (1990).

[34] St. Lenck, J. P. Carbotte, and R. C. Dynes, Phys. Rev. B **50**, 10 149 (1994).

[35] D. Einzel, P. J. Hirschfeld, F. Gross, B. S. Chandrasekhar, K. Andres, H. R. Ott, J. Beuers, Z. Fisk, and J. L. Smith, Phys. Rev. Lett. **56**, 2513 (1986); Z. Phys. B **64**, 175 (1986).

[36] P. Hirschfeld, D. Vollhardt, and P. Woelfle, Solid State Commun. **59**, 111 (1986).

[37] C. J. Pethick and D. Pines, Phys. Rev. Lett. **57**, 118 (1986).

[38] J. Keller, K. Scharnberg, and H. Monien, Physica C **152**, 302 (1988).

[39] R. A. Klemm, K. Scharnberg, D. Walker, and C. T. Rieck, Z. Phys. B **72**, 139 (1988).

[40] J. P. Carbotte, C. Jiang, D. N. Baxov, and T. Timusk, Phys. Rev. B **51**, 11 798 (1995).

[41] D. A. Bonn, S. Kamal, K. Zhang, R. Liang, D. J. Baar, E. Klein, and W. N. Hardy, Phys. Rev. B **50**, 4051 (1994).

[42] K. Ishida, Y. Kitaoka, N. Ogata, T. Kamino, and K. Asayama, Physica C **185-189**, 1115 (1991).

[43] Y. Kitaoka, K. Ishida, G.-q. Zheng, S. Ohsugi, and K. Asayama, J. Phys. Chem. Solid **54**, 1385 (1993).

[44] J. P. Carbotte and C. Jiang, Phys. Rev. B **48**, 431 (1993); **49**, 6126 (1994).

[45] R. Akis, J. P. Carbotte, and T. Timusk, Phys. Rev. B **43**, 12 804 (1991).

[46] W. Lee, D. Rainer, and W. Zimmermann, Physica C **159**, 535 (1989).

[47] N. E. Bickers, D. J. Scalapino, R. T. Collins, and Z. Schlesinger, Phys. Rev. B **42**, 67 (1990).

[48] E. Nicol, J. P. Carbotte, and T. Timusk, Phys. Rev. B **43**, 473 (1991).

[49] F. Marsiglio, R. Akis, and J. P. Carbotte, Phys. Rev. B **45**, 9865 (1992). In this reference, we provide a derivation for the phonon self-energy at $q = 0$, which is almost identical to the conductivity.

[50] S. B. Nam, Phys. Rev. **156**, B470 (1967); **156**, B487 (1967).

[51] O. V. Dolgov, E. G. Maksimov, and S. V. Shulga, in *Electron-Phonon Interaction in Oxide Superconductors*, edited by R. Baquero (World Scientific, Singapore, 1991), p. 30.

[52] C. Jiang and J. P. Carbotte, J. Supercond. **7**, 559 (1994).

[53] W. L. McMillan and J. M. Rowell, in *Superconductivity*, edited by R. D. Parks (Dekker, New York, 1969), p. 561.

[54] J. P. Carbotte, Rev. Mod. Phys. **62**, 1027 (1990).

[55] F. Marsiglio, M. Schossmann, and J. P. Carbotte, Phys. Rev. B **37**, 4965 (1988).

[56] F. Marsiglio, J. P. Carbotte, A. Puchkov, and T. Timusk, Phys. Rev. B **53**, 9433 (1996).

[57] D. Basov *et al.*, Phys. Rev. B **49**, 12 165 (1994).

[58] D. Basov and T. Timusk (private communication).

[59] A. V. Puchkov, T. Timusk, W. D. Mosley, and R. N. Shelton, Phys. Rev. B **50**, 4144 (1994); and (private communication). In this paper, only the real part of the conductivity is shown. The corresponding imaginary part shows the expected structure at twice the gap value.

[60] P. Arberg and J. P. Carbotte, Phys. Rev. B **50**, 3250 (1994).